

Correlation of local structure and electrical activation in arsenic ultrashallow junctions in silicon

Damiano Giubertoni,^{1,a)} Giancarlo Pepponi,¹ Salvatore Gennaro,¹ Massimo Bersani,¹ Mehmet Alper Sahiner,² Stephen P. Kelty,³ Roisin Doherty,⁴ Majeed A. Foad,⁴ Max Kah,⁵ Karen J. Kirkby,⁵ Joseph C. Woicik,⁶ and Piero Pianetta⁷

¹Center for Materials and Microsystems-Fondazione Bruno Kessler, via Sommarive 18, 38050 Povo, Trento, Italy

²Department of Physics, Seton Hall University, South Orange, New Jersey 07079, USA

³Department of Chemistry and Biochemistry, Center for Computational Research, Seton Hall University, South Orange, New Jersey 07079, USA

⁴Front End Products, Applied Materials Inc., 974 E. Arques Avenue, Sunnyvale, California 94085, USA

⁵Surrey Ion Beam Centre, Advanced Technology Institute, Faculty of Engineering and Physical Sciences, University of Surrey, Guildford GU2 7XH, United Kingdom

⁶National Institute of Standards and Technology, Gaithersburg, Maryland 20899, USA

⁷SSRL, 2575 Sand Hill Road, Menlo Park, California 94025, USA

(Received 4 August 2008; accepted 7 October 2008; published online 24 November 2008)

The understanding of the behavior of arsenic in highly doped near surface silicon layers is of crucial importance for the formation of *N*-type ultrashallow junctions in current and future very large scale integrated technology. This is of particular relevance when studying recently developed implantation and annealing methods. Past theoretical as well as experimental investigations have suggested that the increase in As concentration, and therefore the reciprocal proximity of several As atoms, leads to a drastic increase in electrically inactive defects giving only marginal reduction in sheet resistance. Monoclinic SiAs aggregates as well as various arsenic-vacancy clusters contribute to the deactivation of arsenic. This study aims to correlate between the results of electrical activation measurements and x-ray absorption fine structure measurements. Samples were doped with a nominal fluence of 1×10^{15} – 3×10^{15} atoms/cm², implanted at 2 keV, and annealed by rapid thermal treatments, laser submelt treatments, and a combination of both. Hall effect and sheet resistance measurements have been performed to obtain the density of charge carriers. Secondary ion mass spectrometry has been employed to measure the depth profile and the total retained fluences. The percentage of substitutional arsenic has been obtained by least-squares fits of the measured x-ray absorption spectra with simulated spectra of relaxed structures of the defects obtained by density functional theory. A good agreement with the Hall effect measured electrically active dose fraction has been obtained and a quantification of the population of the different defects involved has been attempted. © 2008 American Institute of Physics. [DOI: 10.1063/1.3026706]

I. INTRODUCTION

The use of arsenic as *n*-type dopant in silicon has been extensively investigated and applied for the past and present semiconductor technology. Compared to other *n*-type dopants, arsenic offers a relatively high solid solubility and a high mass that gives low penetration depth when the dopant atoms are introduced by ion implantation. In addition, the low diffusivity minimizes transient enhanced diffusivity compared to phosphorus. Moreover, nonequilibrium annealing processes such as flash or laser annealing (LA) result in levels of As solubility as high as 9.6×10^{21} cm⁻³.¹ However, active As distribution in Si at concentrations higher than 10^{20} cm⁻³ has a tendency to electrically deactivate when subjected to thermal treatment in the 300–750 °C range,^{2–4} even without forming extended precipitates. This was confirmed by Rutherford backscattering spectroscopy^{5,6} [which revealed just slight atom displacement (0.2 Å)],⁷ x-ray standing wave spectroscopy,^{8,9} and transmission electron

microscopy.^{10,11} Several experimental results suggested the clustering around a vacancy of a number of As atoms up to 4 (As_{*n*}V with $n \leq 4$)¹² as the main mechanism responsible for the deactivation. This would explain phenomena associated with As deactivation such as the decrease in coordination number around As atoms measured by extended x-ray absorption fine structure (EXAFS)^{12–14} and the injection of self-interstitials observed on buried boron delta distributions under deactivating As distributions.^{15,16} Formation of dislocation loops in correspondence with the maximum concentration,¹¹ the increase in vacancy number detected by positron annihilation spectroscopy (PAS),¹⁷ and the As atoms surrounding vacancies detected by the combined use of PAS and Doppler broadening^{18–20} are other observations related to arsenic deactivation.

These experimentally based models found more validation from the theoretical calculations reported earlier by Ramamoorthy and Pantelides²¹ and more recently by Mueller *et al.*,²² whose results showed that As₃V and As₄V clusters always have negative formation energies, whereas AsV and As₂V can be thought of as initial steps for deactivation and

^{a)}Electronic mail: giuberto@fbk.eu.

the base of As diffusion through a ring mechanism in a percolation model.^{23,24} DP(2), DP(4), and DP(2)-*V-I* donor pairs have also been proposed as deactivating defects for *n*-type dopants.^{25,26} However, the first two pairs would not be able to account for the injection of self-interstitials observed by Rousseau *et al.*,¹⁶ and their formation energies would always be too high to be relevant according to Mueller *et al.*²² More recently, new theoretical results revealed that an interstitial mediated As diffusion mechanism could foresee activation energies compatible with the measured values.^{27,28} Furthermore, vacancies are easily annihilated by interstitials in the presence of As atoms with a gain of energy >1.3 eV.²⁹ These findings suggest that in the presence of an excess of self-interstitials (*I*), As would remain more favorably as an As_n or As_mI_n complexes rather than As_mV_n . This possible role played by interstitials on As diffusion and deactivation was suggested also by some experimental results.^{30–34}

It is hence evident that the definitive description of mechanisms behind the As deactivation in Si is still uncertain. Moreover, the present and future complementary metal-oxide semiconductor technology for the realization of ultrashallow junctions (USJ) needs dopant distributions confined in the first 20 nm depth with ultimate junction abruptness in order to overcome short-channel effects. This requires levels of electrical activation higher than equilibrium in order to match the specifications of sheet resistance (R_s). These characteristics bring the As distribution to a regime where dopant is expected to deactivate. Furthermore, the USJ requirements are implying the introduction of state of art processes such as ultralow energy implantation, plasma immersion ion implantation, and millisecond thermal treatments like flash or laser melt or submelt annealing, whose junction activation behavior needs to be deeply investigated.

The present study aims to investigate the behavior of distributions of arsenic in ultrashallow regime created in silicon by either rapid thermal annealing or laser submelt annealing using Hall effect measurements, secondary ion mass spectrometry (SIMS), and EXAFS. The latter technique has also been recently applied to investigate the atomic local order around As atoms in USJ.^{35,36} However, after rapid thermal processing (RTP) a large accumulation of disordered or precipitated As is usually created at the surface,^{14,37,35,38} hindering an accurate EXAFS probing of the deeper part of the As distribution. This also affects the discrimination of different levels of local atomic order produced by different thermal processes.³⁶ In a preliminary work, we reported the possibility to remove this As accumulation and to probe the deeper part of the junction.³⁵ In this study, a quantitative interpretation of the EXAFS spectra has been carried out in order to correlate the local atomic order of arsenic to the electrical characteristics as determined by Hall effect measurement. Moreover, the percentage of substitutional dopant produced by the different annealing processes has been obtained through least-squares fits of the EXAFS spectra with simulations of relaxed structures of As_nV defects obtained by density functional theory (DFT). The results confirm EXAFS as a powerful technique, not only able to correlate atomic

structures with macroscopic electrical behaviors but also to give quantitative information about the defect populations even for ultrashallow As distributions.

II. EXPERIMENTAL

P-type (100) Czochralski-silicon wafers have been implanted with As^+ , nominal fluence of 1×10^{15} atoms/cm², implant energy of 2 keV at 0° tilt, and twist angles with an Applied Materials Quantum X implanter. Another wafer was implanted with the same conditions but with 3×10^{15} cm⁻² As^+ fluence. Wafers were annealed in N₂ atmosphere using a production scanning LA system that utilizes a line of solid state lasers under nonmelt conditions. Anneal temperatures were measured using a pyrometer calibrated using a NIST traceable standard, and the laser power was adjusted to achieve a stable temperature to within ± 1 °C. Strips were annealed on each wafer at temperatures of 1150 and 1300 °C. A portion of the remaining as-implanted sample and a portion of the LA sample at 1150 °C were subjected to a RTP at 1050 °C in 10% O₂/90% N₂ atmosphere using Applied Materials RTP Radiance. The diode laser thermal process shows ramp-up and ramp-down rates of about 10⁶ °C/s and the RTP system a ramp up of 250 °C/s and a ramp down of about 90 °C/s. Both thermal processes were spike annealings where the sample was kept between 1000 and 1050 °C for 1.5 s in RTP, whereas LA time was just 1 ms. A part of the samples submitted to the RTP has been etched through several cycles of silicon oxide removal in diluted HF (2% solution) and oxidation in ultrapure water to remove the topmost layer (~2.8 nm for sample 5 and ~4.0 nm for sample 6), where slightly less than half of the arsenic resides after the RTP. Atomic force microscopy measurements on the sample surface before and after etching showed that the etch process has no significant impact on the roughness: the root mean square values were 0.30 nm before etching and 0.24 nm after etching, respectively. A description of the samples and processes can be found in Table I.

The arsenic depth distribution and the total retained fluence for all samples have been determined by SIMS. Measurements have been performed with a CAMECA Wf/SC Ultra with Cs⁺ sputtering at 0.5 keV impact energy and 45° incidence angle, and collection of the ²⁸Si ⁷⁵As⁻ and ²⁸Si₂⁻ secondary ions in high mass resolution. Details of the quantification procedure can be found elsewhere.³⁹ The van der Pauw method was used to measure sheet resistance. The areal “carrier concentration” and mobility results were obtained using Accent HL5500 Hall System. The applied magnetic field of 0.328 T and Hall scattering factor of unity were used.

X-ray absorption fine structure measurements have been performed at room temperature at the BM08 GILDA beamline of the European Synchrotron Radiation Facility in grazing incidence and fluorescence acquisition with a side-looking 13 element GeHP detector. The sample was positioned horizontally.⁴⁰ *K*-edge spectra have been acquired in the energy range of 11600–12700 eV with variable energy step (0.5 eV in the proximity of the edge, 5 eV at the periphery of the scan) at an incidence angle above the critical for

TABLE I. Description and Hall effect results for LA and rapid thermal annealed samples.

Sample ID	Implanted dose (cm ⁻²)	Annealing	Etching	R_s (Ω/sq)	Mobility (cm ² /V s)	Carrier dose (cm ⁻²)	Retained dose (cm ⁻²)	Active fraction (%)
1	1×10^{15}	As implanted	9.6×10^{14}	-
2	1×10^{15}	LA 1150 °C	...	679	31.7	2.9×10^{14}	9.9×10^{14}	29.5
3	1×10^{15}	LA 1300 °C	...	723	32	2.7×10^{14}	1.0×10^{15}	27.3
4	3×10^{15}	LA 1300 °C	...	782	95	9.15×10^{13}	2.7×10^{15}	3.4
5	1×10^{15}	RTP 1050 °C	...	490	64.6	2.0×10^{14}	7.0×10^{14}	28.2
6	1×10^{15}	LA 1150 °C + RTP 1050 °C	...	450	60.8	2.2×10^{14}	6.6×10^{14}	33.6
5 etch	1×10^{15}	RTP 1050 °C	Yes	818	73.4	1.0×10^{14}	3.1×10^{14}	33.2
6 etch	1×10^{15}	LA 1150 °C + RTP 1050 °C	Yes	698	68.7	1.3×10^{14}	3.1×10^{14}	41.9

total reflection (about 0.18° measured from the sample surface) for all samples. The critical angle for total reflection for Si varies between 0.154° and 0.140° for energies in the range of 11600 and 12700 eV, respectively. The chosen angle of incidence allows the sampling of the whole dopant distribution with almost uniform weight across the implant. For samples 5 and 6, spectra have also been acquired at 0.12° (below the critical angle for total reflection and count rates comparable to the measurement at 0.18°) with the aim of sampling only the As atoms in the topmost layer (80% of As fluorescence signal is from the initial ~4 nm for sample 5). A 100 keV As implant (fluence: 1×10^{15} cm⁻²) laser (melting) annealed with supposed electrical activation close to 100% was used as a reference for the EXAFS analyses.

Theoretical EXAFS functions were calculated using University of Washington's multiple scattering XAFS calculation code FEFF8.4.⁴¹ The structural parameters, which were obtained by the DFT calculations, were used in calculating these EXAFS models. The theoretical EXAFS standards for possible cluster structures and monoclinic SiAs precipitates were used in least-square EXAFS fits to the Fourier transformed (FT) data. Experimental EXAFS functions $\chi(k)$'s are extracted by subtracting atomic absorption background using the AUTOBK code.⁴² The $\chi(k)$'s are then FT using a Gaussian window for [2.0–10.0 Å⁻¹] k -range range with a k^2 weighting in order to fully account the contribution from the larger k region. EXAFS fits were performed assuming the copresence of all the As_{*n*}V ($n=1-4$) clusters, SiAs precipitates, and the substitutional As (arsenic atoms surrounded by silicon atoms in silicon crystal) in the samples.

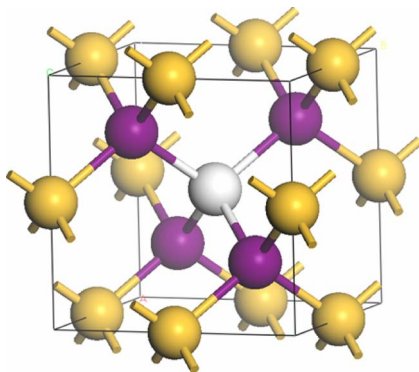


FIG. 1. (Color online) Unit cell schematic showing Si (light), As substitution sites (dark), and Si vacancy (white).

A. Computational details

Geometry optimizations were carried out for four systems containing a Si vacancy surrounded by one to four As substitutional defects using the CASTEP plane wave density functional code.⁴³ Initial state structures of As_{*n*}V (V = vacancy, $n=1-4$) were prepared as follows. A bulk Si crystal ($Fd\bar{3}m$), in which the cell origin was translated by $0.5a$ to place a Si atom at its center, was first relaxed using the GGA PW-91 exchange-correlation functional⁴⁴ to less than 0.01 eV/atom. The plane wave basis cutoff energy was 320 eV, and a Monkhorst–Pack k -point grid with 0.037 Å⁻¹ spacing was used for all energy minimizations. The relaxed Si crystal was modified to contain a Si vacancy defect at the cell center and one to four As substitutional defects in the first coordination shell around the vacancy, Fig. 1. For each defect state the fractional coordinates were optimized using the same functional and convergence criteria as used for bulk Si. The cubic lattice parameters obtained for relaxed bulk Si were used for initial state structures for each of the As substitutional defect states. Geometry optimizations of the defect states were done using fixed lattice parameters but flexible internal fractional coordinates. Fixing the lattice parameters to relaxed bulk values permits geometry optimization of the defect environment while retaining cubic bulk symmetry in the neighboring cells and bulk crystal lattice.

DFT geometry optimizations yielded a Si bulk lattice constant of 5.382 Å, 0.9% smaller than the experimental

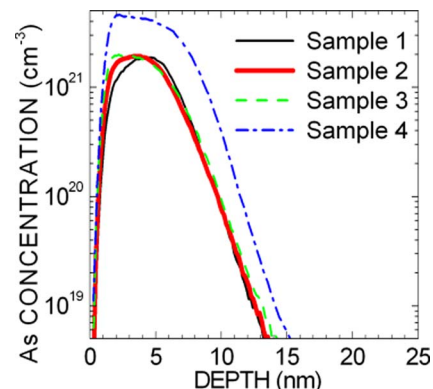


FIG. 2. (Color online) SIMS determined arsenic profiles of as-implanted and LA samples at 1100 and 1300 °C. Sample 1, 1×10^{15} cm⁻² as implanted. Sample 2, 1×10^{15} cm⁻² LA at 1150 °C. Sample 3, 1×10^{15} cm⁻² LA at 1300 °C; Sample 4, 3×10^{15} cm⁻² LA at 1300 °C.

TABLE II. Fractional atomic displacements for geometry optimized As_nV ($n=1-4$) states.

State	a (Å)	Fractional displacement toward vacancy				
Bulk Si	5.382	
AsV	5.382	(As)	(Si)	(Si)	(Si)	
		x	0.0137	0.0051(6)	0.005 16	0.006 12
		y	0.0140	0.0059(5)	0.005 24	0.005 23
		z	0.0140	0.0052(4)	0.005 95	0.005 23
As_2V	5.382	(As)	(As)	(Si)	(Si)	
		x	0.013 77	0.013 77	0.010 83	0.010 83
		y	0.013 77	0.013 77	0.010 83	0.010 83
		z	0.014 51	0.014 54	0.005 12	0.005 12
As_3V	5.382	(As)	(As)	(As)	(Si)	
		x	0.014 00	0.012 66	0.035 78	0.014 59
		y	0.014 33	0.012 66	0.013 73	0.007 93
		z	0.012 50	0.013 78	0.036 07	0.014 88
As_4V	5.382	(As)	(As)	(As)	(As)	
		x	0.017 68	0.017 68	0.017 68	0.017 68
		y	0.017 68	0.017 68	0.017 68	0.017 68
		z	0.017 68	0.017 68	0.017 68	0.017 68

value. DFT geometry optimizations of high atom density crystals, particularly Si, are recognized to yield slightly smaller lattice constants than experimental results although the fractional coordinates are reliable.⁴⁵ The lattice parameters and fractional displacements (in x , y , and z directions) of the atoms in the first coordination shell around the vacancy for optimized As_nV are shown in Table II. In all cases, the vacancy neighbor shell atoms are displaced toward the vacancy on the order of 0.2–0.35 Å for As and 0.1–0.2 Å for Si. Although other vacancy-substitution defects are possible, we modeled those systems that are expected to exhibit the most stable states. Both the stability and diffusion characteristics of these defect states impact their presence in the lattice, particularly after implantation annealing.

III. RESULTS AND DISCUSSION

A. Submelt laser annealed samples

SIMS results shown in Fig. 2 confirmed distribution features already reported for these samples:³⁵ the $1 \times 10^{15} \text{ cm}^{-2}$ “as-implanted” sample has a peak concentration of $1.8 \times 10^{21} \text{ cm}^{-3}$ at 4.3 nm and a measured dose of

$9.6 \times 10^{14} \text{ cm}^{-2}$, i.e., in agreement with the nominal value within measurement error. Subsequent LA induces neither appreciable arsenic outdiffusion nor any relevant dopant indiffusion. The SIMS methodology ensures a good accuracy at the interface between surface SiO_2 and Si, and the only expected inaccuracy would be a shift of the profile to the surface present in all the samples.³⁹ Therefore, we can state that accumulation peaks at the surface SiO_2/Si interface similar to the ones reported for solid phase epitaxial regrowth (SPER) or RTP⁴⁶ are not observed but a slight redistribution in the topmost 5 nm is visible. For this reason the etching process was not applied to these samples before performing EXAFS analysis with the aim of accurately sampling the deeper part of the junction.

Sheet resistance (R_s) values measured on all thermally treated samples are reported in Table I. Samples 2 and 3 showed similar values: 679 and 723 Ω/sq , respectively. Due to the similar junction depth (x_j) observed by SIMS, the R_s difference is expected to be due to a different levels of electrical activation. In fact, the measured active carrier dose is 2.9×10^{14} and $2.7 \times 10^{14} \text{ cm}^{-2}$ for samples 2 and 3, respec-

TABLE III. Active As fraction from Hall effect measurements and fraction of the As complexes obtained from least-squares EXAFS fits.

Sample	Active fraction (%)	X-ray incidence angle	Substitutional As	AsV	As_2V	As_3V	As_4V	SiAs
2	29.5	Above critical angle	0.31	0.10	0.00	0.39	0.14	0.07
3	27.3	Above critical angle	0.26	0.12	0.02	0.53	0.05	0.00
4	3.4	Above critical angle	0.05	0.16	0.05	0.38	0.15	0.21
5	28.2	Above critical angle	0.24	0.06	0.08	0.14	0.18	0.14
		Below critical angle	0.13	0.08	0.16	0.17	0.29	0.17
6	33.6	Above critical angle	0.36	0.09	0.12	0.15	0.14	0.14
		Below critical angle	0.14	0.13	0.17	0.18	0.20	0.18
5 etch	33.2	Above critical angle	0.57	0.04	0.07	0.04	0.20	0.08
6 etch	41.9	Above critical angle	0.58	0.00	0.10	0.08	0.13	0.12
Reference	...	Above critical angle	0.59	0.00	0.24	0.00	0.17	0.00

tively. When the implanted fluence is increased to $3 \times 10^{15} \text{ cm}^{-2}$ the R_s value also appeared to increase to $782 \text{ } \Omega/\text{sq}$ and the active carrier dose decreased to just $9.1 \times 10^{13} \text{ cm}^{-2}$, indicating poorer electrical activation. Due to the accuracy of the SIMS results, the ratio of the Hall effect measured active dose to the SIMS determined dose gives a relatively reliable measure of the active fraction of dopant in the junction: this value, reported in Table I, is nearly one third for the $1 \times 10^{15} \text{ cm}^{-2}$ samples, whereas it falls to $\sim 3\%$ for the $3 \times 10^{15} \text{ cm}^{-2}$ sample. EXAFS was thus used to investigate the amount of As in substitutional position and to understand defects behind the relatively large fractions of inactive dopant. Only As_nV clusters and SiAs precipitates were incorporated in the EXAFS fits together with the substitutional arsenic. As discussed before, As_nV complexes are not the only possible As clusters according to theoretical studies but most likely ones due to lower formation energies. Not only the formation energies but also the diffusion characteristics of different clusters have important effects on the presence of these structures after postimplantation annealing.^{21,22} For As_nV clusters, the local structural parameters obtained from geometry optimization calculations were used in modeling of the EXAFS functions that were used in the least-squares fits. For the monoclinic SiAs, EXAFS modeling the structural parameters from literature was used⁴⁷ and for the substitutional As form, EXAFS model was calculated with arsenic core atom replacing one of the Si atom in a silicon crystal.

FT data of the EXAFS function for the LA samples, measured above critical angle, and the corresponding EXAFS fits except for the as-implanted sample are shown in Fig. 3. The as-implanted data exhibit no long range order beyond the first shell as expected for a high dose amorphizing implant. The final weighting (fraction) of the different structures was determined from the fit results and is listed in Table III. The arsenic coordination numbers, near-neighbor distances, and Debye–Waller factors are listed in Table IV.

Generally the agreement between the active dose obtained from electrical measurement and the fraction of substitutional As obtained with the EXAFS fit results is very good as seen from Table III. The results of the electrical measurements indicate that the application of only LA does not increase activation levels higher than $\sim 30\%$: EXAFS results for the substitutional As fraction for samples 2 and 3 are 33% and 26%, respectively, confirming the findings from combining Hall effect and SIMS characterization. Increasing the As implant dose (sample 3 compared with sample 4) sharply reduces the activated As fraction. Similarly, EXAFS determined substitutional As fraction is significantly lower (5%) for the 3×10^{15} As implant sample. Furthermore, when electrical activation is lower, the coordination number decreases for both first and second shells. The bond length slightly decreases in the first shell whereas increases in the second one; this behavior is consistent with As_nV structures as already reported by Allain *et al.*¹³ and d'Acapito *et al.*³⁶ The latter obtained bond length values systematically slightly higher than the ones reported in Table IV and from Allain but within the experimental error. Regarding the fractions of the As complexes, the low dose samples do not have relevant

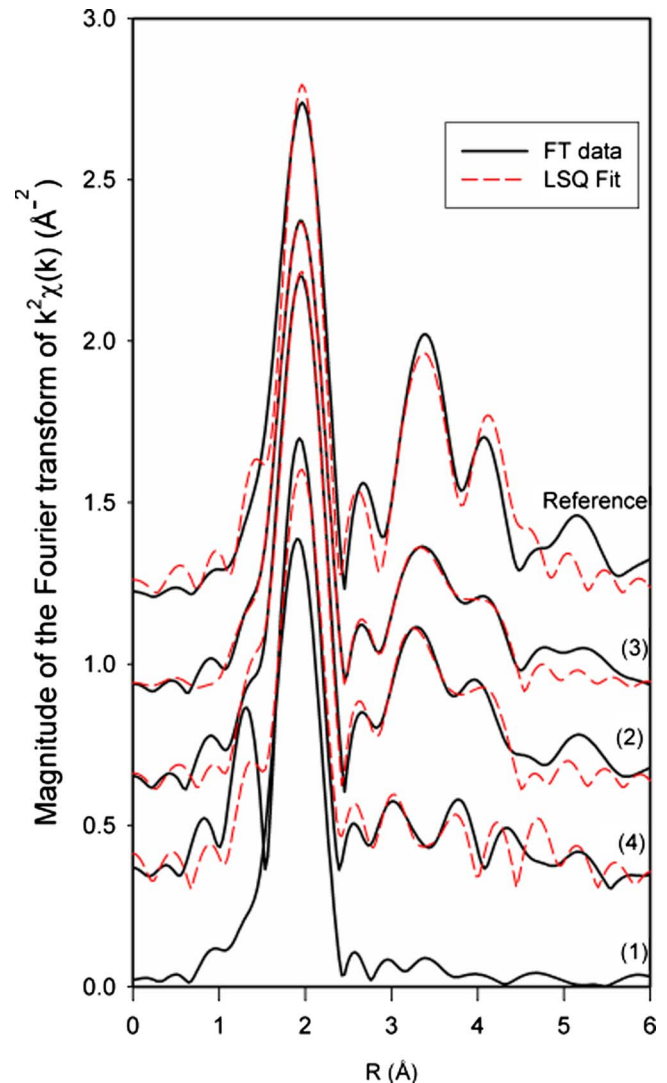


FIG. 3. (Color online) FT EXAFS data and the corresponding fits for LA samples: (1) as implanted, (2) $1 \times 10^{15} \text{ cm}^{-2}$ LA $1150 \text{ }^\circ\text{C}$, (3) $1 \times 10^{15} \text{ cm}^{-2}$ LA $1300 \text{ }^\circ\text{C}$, and (4) $3 \times 10^{15} \text{ cm}^{-2}$ LA $1300 \text{ }^\circ\text{C}$. The reference sample and the as-implanted sample (data only) were plotted for comparison purposes of the second shell structures.

presence of SiAs precipitates, but most As is in As_nV and As_3V defects. The latter prevails as main deactivating defect even on the more thermodynamically stable As_4V , probably because of kinetics constraints and because entropy does not favor the formation of large complexes in line with what is suggested by Mueller *et al.*²² When the As dose is increased (sample 4), the fractions of dopant in As_4V and SiAs complexes increase as expected, due to the higher concentration.

B. RTP annealed samples

SIMS measurements carried out on the two RTP treated samples (5 and 6) are reported in Fig. 4. The results confirmed previously found³⁵ similar distribution features, i.e., a peak of arsenic near the surface, a deeper diffused tail with a box shape, similar junction depth, and an overall $\sim 30\%$ decrease in the retained fluence, probably due to the annealing atmosphere not able to prevent As outdiffusion. However, new more accurate results revealed a lower difference in retained fluence between the two samples with respect to those

TABLE IV. Coordination numbers, near-neighbor distances, and Debye–Waller factors from EXAFS fits.

Sample ID	X-ray incidence angle	First shell			Second shell		
		N	R (Å)	σ (Å ²)	N^*	R (Å)	σ (Å ²)
2	Above critical angle	3.7(2)	2.38(2)	0.002(1)	10.8(4)	3.85(2)	0.04(1)
3	Above critical angle	3.6(2)	2.37(2)	0.002(1)	11.3(3)	3.87(2)	0.03(1)
4	Above critical angle	3.3(2)	2.36(2)	0.004(2)	9.9(4)	3.88(2)	0.05(3)
5	Above critical angle	3.7(3)	2.38(2)	0.003(2)	10.6(3)	3.86(2)	0.04(2)
	Below critical angle	3.4(3)	2.35(1)	0.003(2)	10.3(4)	3.87(1)	0.03(2)
6	Above critical angle	3.6(3)	2.38(2)	0.002(1)	10.6(3)	3.85(2)	0.02(2)
	Below critical angle	3.5(2)	2.36(1)	0.003(1)	10.2(4)	3.88(2)	0.04(2)
5 etch	Above critical angle	3.8(2)	2.39(2)	0.002(1)	11.5(2)	3.85(1)	0.03(2)
6 etch	Above critical angle	3.8(2)	2.39(2)	0.002(1)	11.4(2)	3.85(1)	0.03(2)
Reference	Above critical angle	3.9(1)	2.40(1)	0.002(1)	11.6(2)	3.84(1)	0.02(1)

previously reported, i.e., 7.0×10^{14} and 6.6×10^{14} cm⁻² for samples 5 and 6, respectively. In the Hall effect results, Table I, a higher R_s value is measured for sample 5 (RTP) compared to sample 6 (laser and RTP), 490 against 450 Ω /sq, respectively. The active carrier fluence, however, is higher for sample 6, 2.2×10^{14} against 2.0×10^{14} of sample 5. Consequently, the determined active dose fraction is 28% and 34% for samples 5 and 6, respectively. This is coherent with the difference in R_s values, given the same junction depth for the two samples.

The accumulation of As below the surface oxide following RTP or SPER annealing is well known in literature.^{38,46,48} This arsenic accumulation is often constituted of As in either a disordered form or in SiAs precipitates,^{10,37} and it can hinder the probing of the deeper part of the junction in an x-ray absorption experiment using grazing incidence.³⁵ Therefore, the etching process was tested on these samples as described in Sec. II. SIMS profiles obtained on the etched samples are reported in Fig. 4, shifted by 2.8 and 4.0 nm, respectively, in order to match the As tail.

FT of EXAFS function for these samples together with the relative fits are depicted in Fig. 5 for measurements carried out above and below critical angle for the unetched samples, only above critical angle for the etched ones. The results of the analysis are summarized in Tables III and IV.

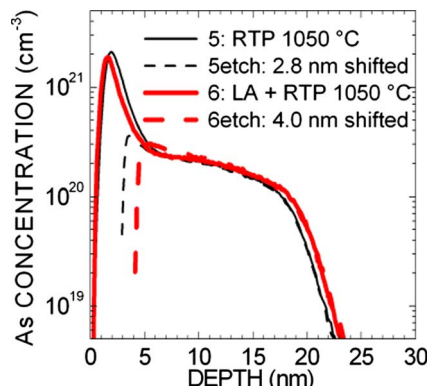


FIG. 4. (Color online) Arsenic SIMS profiles before and after etch for samples with RTP and LA followed by RTP. The etched sample SIMS profiles were rigidly shifted to match the As tail as depicted in the figure in order to know how much As was removed.

All the measurements revealed very similar values for number of coordination and bond length in the first and second shells between samples 5 and 6: The absolute values for bond length reproduce the ones obtained by Allain *et al.*¹³ on As distributions with similar coordination number in the first shell, whereas they are systematically lower than the more recently published by d'Acapito *et al.*³⁶ This discrepancy

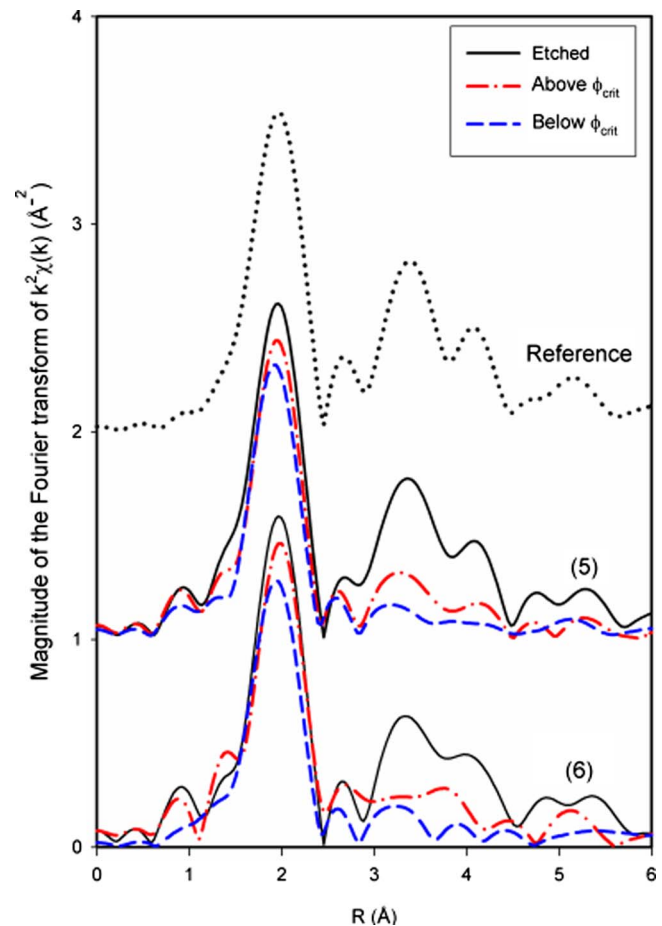


FIG. 5. (Color online) FT EXAFS data for the RTP and the LA+RTP sample. (5) 1×10^{15} cm⁻² RTP 1050 °C. (6) 1×10^{15} cm⁻² LA 1150 °C +RTP 1050 °C. FT data for the etched samples, and above and below critical angle measurements, were shown with the reference samples for comparison purposes.

might be due to differences in the implant energies used in this work (2 keV) and the ones used in the work of d'Acapito *et al.*³⁶ (5 keV). In the lower energy implants one would expect to have a higher As peak concentration close to surface where the near neighbor distances tend to go to lower values.^{14,37}

However, when probing the topmost layer with an incident angle below critical, coordination number and bond length of the first shell decrease compared to the above critical angle results as well as to the values observed on the only LA samples. This would denote a higher presence of vacancies near As atoms and thus a poorer substitutionality. On the other hand, when etched samples are analyzed, those parameters are very close to the ones obtained on the highly activated reference.

Regarding the fraction of As in the different complexes, the higher values for the substitutional As fraction have been found for sample 6, to which both LA and RTP have been applied, in agreement with the Hall effect result. Furthermore, in measurements carried out at primary beam incidence below the critical angle, the As substitutional fraction falls to $\sim 13\%$ for both samples, indicating that the As in the topmost layer is mostly off lattice sites. On the other hand, when the etched samples are probed, the same fraction increases to $\sim 60\%$. If this factor is applied to the total retained doses as measured by SIMS ($\sim 3.1 \times 10^{14} \text{ cm}^{-2}$ for both samples), the total As in substitutional position is $1.8 \times 10^{14} \text{ cm}^{-2}$, that is nearly the same as that measured above critical angle (probing the whole dopant distribution) on sample 5 ($1.7 \times 10^{14} \text{ cm}^{-2}$) and slightly less than sample 6 ($2.4 \times 10^{14} \text{ cm}^{-2}$), probably because the latter was etched more than sample 5. This means that the active dopant is mainly located in the box-shaped tail, whereas in the accumulation close to the surface (top 2.5 nm), where As concentration is high ($> 2 \times 10^{21} \text{ cm}^{-3}$), the clustering and precipitation of As are expected. In fact, the fraction of As in the deactivating defects As_nV and SiAs increases when samples are probed below critical angles, especially As_3V , As_4V , and SiAs. The As_4V and SiAs population is higher than what is observed in the LA $1 \times 10^{15} \text{ cm}^{-2}$ samples. This is argued to be due to the higher As concentration created at the surface by the RTP induced diffusion. Moreover, the same effect moved dopant atoms, favoring the formation of more stable complexes and overcoming the kinetics constraints. On the other hand, in the etched samples, all the As_nV complex fractions are very low except for As_4V and SiAs ones. In any case, in absolute values, the latter corresponds to $3\text{--}6 \times 10^{13} \text{ As/cm}^{-2}$, i.e., just $\sim 40\%$ of what is observed in the surface layer. The biggest discrepancy between Hall effect active fraction and EXAFS determined As substitutional fraction was found on the etched samples. The reason is under investigation at the moment, but it can be supposed to be related to artifacts induced by the etching process.

A detailed investigation on the correlation between various heat treatments and EXAFS determined fractions of the As clusters and the correlation between the theoretically calculated parameters (such as formation energies and diffusion properties) will be performed in the future.

IV. CONCLUSION

Electrically active As concentration and local structure around the As atom have shown good correlation in a series of As implants in Si subjected to various postimplantation heat treatments. The As atoms were implanted at an energy of 2 keV with doses between 1×10^{15} and $3 \times 10^{15} \text{ cm}^{-2}$, and then annealed by either laser submelting treatment or RTP. The active carrier concentration from Hall effect measurements was correlated with the substitutional As determined by the EXAFS least-squares fits performed by using DFT calculated theoretical standards for the As_nV cluster forms and monoclinic SiAs precipitates. Fractions of the SiAs precipitates and the other As_nV clusters were determined from the EXAFS results. A strong correlation was observed between the EXAFS results and the electrical results in terms of active carrier concentration and the substitutional As. The only laser treatment produced less than a third of active As on the $1 \times 10^{15} \text{ cm}^{-2}$ samples. The $\sim 70\%$ inactive dopant is mainly confined in As_3V complexes as expected from theoretical considerations. In fact, the As_4V complex is more stable but kinetics constraints hinder its formation. However, when the As dose is increased to $3 \times 10^{15} \text{ cm}^{-2}$ the electrically active fraction falls to less than 5% and As is found also in As_4V and SiAs precipitates. RTP processing induced a relevant As indiffusion and an accumulation of As in a thin layer below the surface oxide. The combined use of results obtained by varying primary x-ray beam angle and using a surface etched sample enabled us to conclude that 24% of the As implanted dose is essentially confined below the surface accumulation. The latter is mainly formed by As_3V , As_4V , and SiAs complexes. LA followed by RTP led to pronounced As atom redistribution, resulting also in the highest active carrier concentration (34%) as determined from electrical measurements. EXAFS results indicated 36% of substitutional As for the same sample.

ACKNOWLEDGMENTS

The authors would like to acknowledge Francesco d'Acapito, INFN, and ESRF Grenoble for support and discussion during EXAFS analysis session, Silvia Milita, CNR-IMM Bologna for providing reference sample and helping during EXAFS analysis, and Justin Hamilton and Jim Sharp, University of Surrey for characterizing some samples by Hall Effect measurements. The work of M.A.S. is supported by Research Corporation Award No. CC6405 and NSF Grant No. DMI 0420952. We acknowledge the support of the European Commission under the action 'Structuring the European Research Area'. NIST disclaimer: Certain commercial equipment, instruments, or materials are identified in this document. Such identification does not imply recommendation or endorsement by the National Institute of Standards and Technology, nor does it imply that the products identified are necessarily the best available for the purpose.

¹R. Duffy, T. Dao, Y. Tamminga, K. van der Tak, F. Roozeboom, and E. Augendre, *Appl. Phys. Lett.* **89**, 071915 (2006).

²R. O. Schwenker, E. S. Pan, and R. F. Lever, *J. Appl. Phys.* **42**, 3195 (1971).

- ³A. Lietoila, J. F. Gibbons, T. J. Magee, J. Peng, and J. D. Hong, *Appl. Phys. Lett.* **35**, 532 (1979).
- ⁴D. Nobili, S. Solmi, A. Parisini, M. Derdour, A. Armigliato, and L. Moro, *Phys. Rev. B* **49**, 2477 (1994).
- ⁵A. Lietoila, J. F. Gibbons, and T. W. Sigmon, *Appl. Phys. Lett.* **36**, 765 (1980).
- ⁶C. Brizard, J. R. Regnard, J. L. Allain, A. Bourret, M. Dubus, A. Armigliato, and A. Parisini, *J. Appl. Phys.* **75**, 126 (1994).
- ⁷A. Satta, E. Albertazzi, G. Lulli, and L. Colombo, *Phys. Rev. B* **72**, 235206 (2005).
- ⁸A. Herrera-Gomez, P. M. Rousseau, G. Materlik, T. Kendelewicz, J. C. Woicik, P. B. Griffin, J. Plummer, and W. E. Spicer, *Appl. Phys. Lett.* **68**, 3090 (1996).
- ⁹A. Herrera-Gómez, P. M. Rousseau, J. C. Woicik, T. Kendelewicz, J. Plummer, and W. E. Spicer, *J. Appl. Phys.* **85**, 1429 (1999).
- ¹⁰A. Parisini, A. Bourret, A. Armigliato, M. Servidori, S. Solmi, R. Fabbri, J. R. Regnard, and J. L. Allain, *J. Appl. Phys.* **67**, 2320 (1990).
- ¹¹O. Dokumaci, P. M. Rousseau, S. Luning, V. Krishnamoorthy, K. S. Jones, and M. E. Law, *J. Appl. Phys.* **78**, 828 (1995).
- ¹²K. C. Pandey, A. Erbil, G. S. Cargill III, R. F. Boehme, and D. Vanderbilt, *Phys. Rev. Lett.* **61**, 1282 (1988).
- ¹³J. L. Allain, J. R. Regnard, A. Bourret, A. Parisini, A. Armigliato, G. Tourillon, and S. Pizzini, *Phys. Rev. B* **46**, 9434 (1992).
- ¹⁴M. A. Sahiner, S. W. Novak, J. Woicik, J. Liu, and V. Krishnamoorthy, *IEEE Transactions Ion Implantation Technology*, 2000 (unpublished), Vol. 00EX432, p. 600.
- ¹⁵P. M. Rousseau, P. B. Griffin, and J. D. Plummer, *Appl. Phys. Lett.* **65**, 578 (1994).
- ¹⁶P. M. Rousseau, P. B. Griffin, W. T. Fang, and J. D. Plummer, *J. Appl. Phys.* **84**, 3593 (1998).
- ¹⁷D. W. Lawther, U. Myler, P. J. Simpson, P. M. Rousseau, P. B. Griffin, and J. D. Plummer, *Appl. Phys. Lett.* **67**, 3575 (1995).
- ¹⁸U. Myler, P. J. Simpson, D. W. Lawther, and P. M. Rousseau, *J. Vac. Sci. Technol. B* **15**, 757 (1997).
- ¹⁹K. Saarinen, J. Nissila, H. Kauppinen, M. Hakala, M. J. Puska, P. Hautolarvi, and C. Corbel, *Phys. Rev. Lett.* **82**, 1883 (1999).
- ²⁰V. Ranki, A. Pelli, and K. Saarinen, *Phys. Rev. B* **69**, 115205 (2004).
- ²¹M. Ramamoorthy and S. T. Pantelides, *Phys. Rev. Lett.* **76**, 4753 (1996).
- ²²D. C. Mueller, E. Alonso, and W. Fichtner, *Phys. Rev. B* **68**, 045208 (2003).
- ²³D. Mathiot and J. C. Pfister, *Appl. Phys. Lett.* **42**, 1043 (1983).
- ²⁴J. Xie and S. P. Chen, *Phys. Rev. Lett.* **83**, 1795 (1999).
- ²⁵D. J. Chadi, P. H. Citrin, C. H. Park, D. L. Adler, M. A. Marcus, and H.-J. Gossman, *Phys. Rev. Lett.* **79**, 4834 (1997).
- ²⁶P. M. Voyles, D. J. Chadi, P. H. Citrin, D. A. Muller, J. L. Grazul, P. A. Northrup, and H.-J. L. Gossmann, *Phys. Rev. Lett.* **91**, 125505 (2003).
- ²⁷S. A. Harrison, T. F. Edgar, and G. S. Hwang, *Appl. Phys. Lett.* **87**, 231905 (2005).
- ²⁸S. A. Harrison, T. F. Edgar, and G. S. Hwang, *Phys. Rev. B* **74**, 195202 (2006).
- ²⁹S. A. Harrison, T. F. Edgar, and G. S. Hwang, *Appl. Phys. Lett.* **85**, 4935 (2004).
- ³⁰R. Brindos, P. Keys, K. S. Jones, and M. E. Law, *Appl. Phys. Lett.* **75**, 229 (1999).
- ³¹R. Kim, T. Hirose, T. Shano, H. Tsuji, and K. Taniguchi, *Jpn. J. Appl. Phys., Part 1* **41**, 227 (2002).
- ³²S. Solmi, M. Ferri, M. Bersani, D. Giubertoni, and V. Soncini, *J. Appl. Phys.* **94**, 4950 (2003).
- ³³N. Kong, S. K. Banerjee, T. A. Kirichenko, S. G. H. Anderson, and M. C. Foisy, *Appl. Phys. Lett.* **90**, 062107 (2007).
- ³⁴N. Kong, T. A. Kirichenko, Y. Kim, M. C. Foisy, and S. K. Banerjee, *J. Appl. Phys.* **104**, 013514 (2008).
- ³⁵D. Giubertoni, G. Pepponi, M. Bersani, S. Gennaro, F. D'Acapito, R. Doherty, and M. A. Foad, *Nucl. Instrum. Methods Phys. Res. B* **253**, 9 (2006).
- ³⁶F. d'Acapito, S. Milita, A. Satta, and L. Colombo, *J. Appl. Phys.* **102**, 043524 (2007).
- ³⁷A. Terrasi, E. Rimini, V. Raineri, F. Iacona, F. La Via, S. Colonna, and S. Mobilio, *Appl. Phys. Lett.* **73**, 2633 (1998).
- ³⁸R. Kasnavi, Y. Sun, R. Mo, P. Pianetta, P. B. Griffin, and J. D. Plummer, *J. Appl. Phys.* **87**, 2255 (2000).
- ³⁹D. Giubertoni, M. Bersani, M. Barozzi, S. Pederzoli, E. Iacob, J. A. van den Berg, and M. Werner, *Appl. Surf. Sci.* **252**, 7214 (2006).
- ⁴⁰G. Pepponi, D. Giubertoni, S. Gennaro, M. Bersani, M. Anderle, R. Grisenti, M. Werner, and J. A. van den Berg, in *Ion Implantation Technology*, Marseille, France, edited by K. J. Kirkby, R. Gwilliam, A. Smith, and D. Chivers (AIP, New York, 2006), Vol. 117.
- ⁴¹A. L. Ankudinov, B. Ravel, J. J. Rehr, and S. D. Conradson, *Phys. Rev. B* **58**, 7565 (1998).
- ⁴²M. Newville, P. Livins, Y. Yacoby, J. J. Rehr, and E. A. Stern, *Phys. Rev. B* **47**, 14126 (1993).
- ⁴³M. D. Segall, P. J. D. Lindan, M. J. Probert, C. J. Pickard, P. J. Hasnip, S. J. Clark, and M. C. Payne, *J. Phys.: Condens. Matter* **14**, 2717 (2002).
- ⁴⁴J. P. Perdew and Y. Wang, *Phys. Rev. B* **45**, 13244 (1992).
- ⁴⁵C. Skylaris and P. D. Haynes, *J. Chem. Phys.* **127**, 164712 (2007).
- ⁴⁶A. Parisini, V. Morandi, S. Solmi, P. G. Merli, D. Giubertoni, M. Bersani, and J. A. van den Berg, *Appl. Phys. Lett.* **92**, 261907 (2008).
- ⁴⁷T. Wadsten, *Acta Chem. Scand.* **19**, 1232 (1965).
- ⁴⁸K. Suzuki, Y. Kataoka, S. Nagayama, C. W. Magee, T. H. Buyuklimanli, and T. Nagayama, *IEEE Trans. Electron Devices* **54**, 262 (2007).